Nano Energy 92 (2022) 106778

Contents lists available at ScienceDirect

Nano Energy

journal homepage: www.elsevier.com/locate/nanoen

On-wire axial perovskite heterostructures for monolithic dual-wavelength laser

Pengfei Guo [a,b,*], Da Liu [a], Xia Shen [a], Qihang Lv [a], Yu Wu [a], Qian Yang [a], Pu Li [a], Yuying Hao [a], Johnny C. Ho [c,d,**], Kin Man Yu [b,***]

[a] College of Physics and Optoelectronics, Key Laboratory of Advanced Transducers and Intelligent Control System Ministry of Education, Taiyuan University of Technology, Taiyuan 030024, China
[b] Department of Physics, City University of Hong Kong, Kowloon 999077, Hong Kong, China
[c] Department of Materials Science and Engineering, City University of Hong Kong, Kowloon 999077, Hong Kong, China
[d] Institute for Materials Chemistry and Engineering, Kyushu University, Fukuoka 816-8580, Japan

ARTICLE INFO

Keywords:
Perovskite
Heterostructure
On-wire bandgap integration
Asymmetric waveguide
Dual-wavelength lasing

ABSTRACT

All-inorganic lead halide perovskites have attracted tremendous attention for their tunable bandgaps, excellent photoluminescence efficiency and robust stability. Here, we report on a direct vapor-phase growth of high-quality $CsPbCl_3/CsPbI_3$ axial perovskite heterostructure and multi-heterojunction nanowires using a newly developed magnetic-pulling chemical vapor deposition approach. Microstructural characterization and optical investigations reveal that these structures are crystalline with abrupt heterojunctions. Micro-photoluminescence spectra and mapping at the heterojunctions exhibit dual-wavelength emissions at 417 nm and 698 nm, from the adjacent two disparate perovskites, respectively, further demonstrating the formation of unique heterostructures. Additionally, under a focused laser illumination, asymmetrical waveguide behavior along a single $CsPbCl_3/CsPbI_3$ wire is clearly observed. Taking a step further, we fabricated a monolithic dual-wavelength laser using an on-wire axial perovskite heterostructure and successfully realized blue and red emissions (425.5 nm and 687.4 nm). The capability to synthesize on-wire heterostructures represents a major step toward high-integration optoelectronic circuits and nanophotonics.

1. Introduction

Inorganic lead halide perovskite materials have attracted tremendous attention owing to their versatile physical/chemical characteristics, which make them promising candidate material platforms for next-generation optoelectronic circuits [1–9]. In particular, rational constitution and controllable design of the bandgaps on perovskite nanostructures are vitally essential in yielding enriched and/or improved multifunctionalities for their applications in high-performance optoelectronic and nanophotonic devices [10–17]. Significant research efforts are currently directed toward the tunable band-edge emission of lead halide-based perovskites owing to their outstanding characteristics [4,18–25]. For example, wavelength tunable lasing of bandgap engineered halide perovskite nanostructures are reported by a vapor growth process [7,22,26,27]. $CsPb_xSn_{1-x}I_3$ alloy perovskite nanowires are systematically studied through a phase transition process [28]. Organic-inorganic hybrid perovskite nanowire/nanocrystal laser arrays are realized using a template assisted "bottom-up" self-assembly method [29,30]. $CsPbX_3$ quantum dots and $CH_3NH_3PbX_3$ nanoplatelets are reported to establish high-efficiency light emitting diodes [31,32]. Nano-heterostructures with dual-emission wavelength are routinely fabricated by anion-exchange process, ion doping, and phase transition et al. [13,33–35]. Especially, perovskite heterojunctions and thin films grown via a solution-based synthetic route with selective anion-exchange process, may help to guide the growth of large-area monocrystalline heterostructure arrays [33]. Additionally, a phenomenon of spinodal decomposition is reported to realize epitaxial mixed halide perovskites heterostructures [34]. Reduced electron-phonon

* Corresponding author at: College of Physics and Optoelectronics, Key Laboratory of Advanced Transducers and Intelligent Control System Ministry of Education, Taiyuan University of Technology, Taiyuan 030024, China.
** Corresponding author at: Department of Materials Science and Engineering, City University of Hong Kong, Kowloon, 999077, Hong Kong, China.
*** Corresponding author.
E-mail addresses: guopengfei@tyut.edu.cn (P. Guo), johnnyho@cityu.edu.hk (J.C. Ho), kinmanyu@cityu.edu.hk (K.M. Yu).

https://doi.org/10.1016/j.nanoen.2021.106778
Received 16 September 2021; Received in revised form 21 November 2021; Accepted 22 November 2021
Available online 27 November 2021

coupling was discovered in these heterjunctions, which may owe to the classic phonon confinement effect. Despite all this extraordinary progress, these reported schemes for multi-color emissions to date often suffer from complex preparation route, costly large-scale promotion, and high operation threshold intensity, which may seriously hinder their further applications.

Compared to one-dimensional homogeneous nanowires, heterostructure wires with expanded absorption bands and enhanced light-matter interactions are expected to serve as double gain materials, bidirectional optical transmission medium, and dual-oscillating cavities, because of their multi-component structure and high refractive index contrast to the surroundings [36–38]. Moreover, asymmetric optical transmission process has not yet been realized in homogeneous perovskite nanostructures for the challenge of breaking time reversal symmetry of light-matter interaction [39–42]. However, to the best of our knowledge, vapor-phase growth of on-wire multi-functional perovskite heterostructures with spatially resolved emissions with multi-wavelength are rarely reported, which may be plagued by the poor controllability of the solid evaporation sources under high temperature. In this work, we report on the design and realization of a direct vapor-phase growth of high-quality axial halide perovskite heterostructures using a developed magnetic-pulling chemical vapor deposition (CVD) approach. This strategy is capable of on-wire fabrication of perovskite heterostructures, and overcomes the poor controllable synthesis against the disparate component on a single nanowire under high temperature. Structural characterization reveals that these on-wire perovskite heterostructures have high crystalline quality. Spatially micro-photoluminescence (μ-PL) spectra and mapping indicate two separated narrow emission bands at 417 nm and 698 nm along the axial direction of heterojunctions. Asymmetrical waveguides with active and passive behaviors along the axial directions are demonstrated under a focused laser illumination on these unique axial $CsPbCl_3/CsPbI_3$ nanostructures. Furthermore, a monolithic dual-wavelength laser with a blue (425.5 nm) and red (687.4 nm) emission lines using an on-wire axial perovskite heterostructure is successfully realized. The preparation of on-wire $CsPbCl_3/CsPbI_3$ heterostructures and multi-heterojunction nanowires may also have potential applications for photovoltaics and solid-state lighting in the future.

2. Experimental section

2.1. Material preparation

The $CsPbCl_3/CsPbI_3$ axial heterostructure nanowires were grown via a temperature controlled multi-step CVD strategy, as schematically shown in Fig. S1 (See Supporting Information). Sources and reagents were purchased from Alfa Aesar. A horizontal furnace (OTF-1200X) with a 2-inch quartz tube (inner diameter 45 mm, length 180 cm) was used. Before the growth, two alumina boats with $CsCl/PbCl_2$ and CsI/PbI_2 were mixed in their respective boat (mole ratio = 2:1), and they were placed in the center and upstream of the heating zone, respectively, and were separated by a quartz rod and located far enough away from each other. A quartz rod driven by step motor through magnetic force was used to push these boats into/out of the heating zone during the growth. Several piece of Si/SiO_2 (4 mm × 10 mm) were placed at the deposition area. Before heating, dry N_2 gas flow was introduced into the system at a rate of 60 sccm for 30 min to purge the oxygen and moisture from the tube. After that, H_2 (35 sccm) flow was introduced into the system, while the pressure in the tube was maintained at 3.8 Torr. The temperature in the left and right zones were ramped up to 610 °C and 580 °C at a rate of 25 °C min^{-1}, respectively. After 40 mins, the temperature in the left zone was reduced at a rate of 15 °C min^{-1} to 580 °C. The second boat (CsI/PbI_2) was quickly pushed into the left zone to replace the former boats at a rate of 20 cm min^{-1} by a stepping motor. Then the gas flow (N_2, 40 sccm; H_2, 35 sccm) was slightly changed. The temperature was kept for an addition 20–40 min while maintaining the pressure at 1.5 Torr. After the growth, the furnace was naturally cool to 25 °C. For the multi-heterojunction nanowires, the pressure is maintained at 3.5 torr, and the gas flow is H_2 (60 sccm)/N_2 (50 sccm). As shown in Fig. S2 (See Supporting Information), it is important to point out that the right zone was first ramped up to 460 °C before growth, in which the substrates were located. Then the temperature in the left zone was ramped to 570 °C. After the first step, the temperature of the two zones were decreased to 515 °C and 400 °C, respectively.

2.2. Characterization

The morphology and chemical composition of the perovskite heterostructure nanowires were investigated via scanning electron microscopy (SEM, Hitachi, S-4800, Japan) with energy dispersive x-ray spectroscopy capability at an accelerating voltage of 5.0 kV, and transmission electron microscopy (TEM, JEM-F200). The crystal structures were determined by X-ray diffraction (Bruker D8). The far-field optical images, PL spectra and mapping were obtained by a home-built confocal optical system. A laser beam was focused (375 nm, spot size, 1.5 μm) by a microscope lens (Nikon, ×100) and locally excited at the heterostructures. The PL spectra were recorded by a Ocean Optics Spectrometer (Maya Pro2000). Stimulated emission properties were performed by another confocal optical system. The nanowires were selected and transferred to a MgF_2 substrate or a copper grid by a 3D manipulator with homemade fiber probes for characterization, as schematically shown in Fig. S3 (See Supporting Information). A Ti:sapphire pulsed laser (400 nm, 150 fs, 1KHz) was focused to 50 μm and then pumped widely onto the nanowires. The PL spectra were recorded by Ocean Optics Spectrometer (LBS2500).

3. Results and discussion

Low- and high-resolution scanning electron microscopy (SEM) images reveal that, in general, nanowires synthesized by a conventional magnetic-pulling CVD method (Fig. S1, See Supporting Information) have a non-uniform linear morphology with lengths of 10–20 micrometers and diameter ranging from 100 to 500 nm (Fig. 1A and B). Fig. S4A–C (See Supporting Information) show SEM images of three typical wires randomly picked from the as-prepared substrate. It is observed that catalyst seeds are clearly witnessed at the tip of the wires, which indicates that these wires are prepared via a vapor-liquid-solid (VLS) mechanism. Notably, the diameter of wires changed slightly from wire to wire, which may be caused by the pressure variation during the precursor source moving process between the two growth steps. Fig. S4D (See Supporting Information) exhibits an X-ray diffraction (XRD) pattern of these nanostructures, which can be indexed to the tetragonal and orthorhombic phases from $CsPbCl_3$ and $CsPbI_3$ segments, respectively.

The compositional uniformity and variation along the nanowires are then evaluated by energy-dispersive X-ray spectroscopy (EDX) mapping. Fig. 1C shows a typical SEM image of a representative $CsPbCl_3/CsPbI_3$ nanowire heterostructure with the length of ~8 μm. Fig. 1D displays the enlarged SEM image of the heterojunction area (red rectangle), from which an abrupt interface with two different components ($CsPbCl_3$ and $CsPbI_3$) along the junction can been seen. Unfortunately, due to the large diameter (~265 nm) of the nanowire, high-resolution TEM images cannot be performed along the wires. Fig. 1E shows the elemental maps along the axial direction of the wire depicted in Fig. 1C. The results reveal that the wire tip primarily consists of Pb with a small amount of Sn, in agreement with the EDX spectrum of the wire-tip shown in Fig. S5 (See Supporting Information). Along the entire nanowire, the distribution of Pb and Cs are rather uniform. However, at the junction, the I signal abruptly end, while the Cl signal appears, suggesting the formation of an abrupt $CsPbI_3/CsPbCl_3$ heterojunction here. Fig. 1F shows EDX spectra collected from three representative positions along the wire (dots 1–3 in Fig. 1C). The EDX spectrum of position 1 shows the

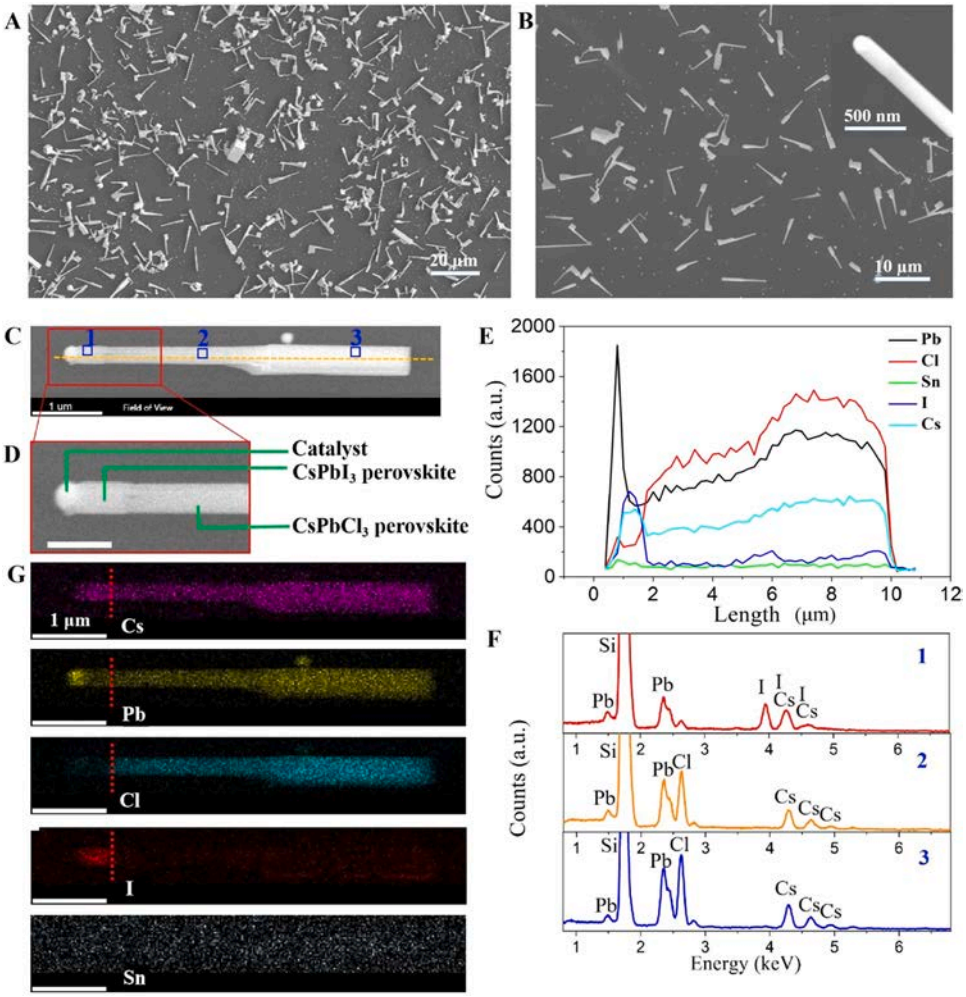

Fig. 1. Compositional analysis of the $CsPbCl_3$/$CsPbI_3$ perovskite heterojunction nanowires. (A,B) Low- and high-resolution SEM images of as-growth $CsPbCl_3$/$CsPbI_3$ heterostructure nanowires. Inset in (B): top-view SEM image of a selected heterostructure with a catalyst on the wire's tip. (C) A SEM image of a single heterostructure nanowire. (scale bar, 1 μm) (D) Enlarged section of the SEM image in (C) showing the abrupt interface along the junction in the nanowire. (scale bar, 500 nm) (E) Elemental composition profiles showing the distribution of the various elements along the axial direction of the wire (dotted line shown in (C)) as obtained by EDX measurements. (F) 2D EDX elemental mapping of the heterostructure nanowire. (G) EDX spectra taken at three typical positions (positions 1–3) along the wire length as indicated in (C).

existence of Pb, Cs, and I with the negligible Cl signal, while only Pb, Cs, and Cl signals are present in the spectra from position 2 and 3. It is worth to note that the atoms are slightly more presented at the thicker part of the nanowire, which is owing to the diameter difference. In order to clearly display the spatial element distributions, a two dimensional (2D) elemental mapping of the wire are shown in Fig. 1G for the detected elements of Pb, Cs, I, and Cl. Evidently, I is located only in the left part of the wire with Cl almost completely distributed in right part of the wire, while Cs and Pb are very homogeneously distributed along the whole body of the wire. Besides, the wire tip (catalyst) has a Pb rich distribution. Sn is homogeneously distributed on the entire substrate. The elemental analysis result demonstrates that these nanowires are actually heterojunctions with $CsPbI_3$ compound on one segment and $CsPbCl_3$ compound on the other, which is also consistent with the observations in real color photographs and μ-PL spectra presented in Fig. S6 (See Supporting Information).

Top-view real-color photograph of a heterojunction nanowire under a wide illumination of continuous wave (CW) laser at 375 nm is exhibited in Fig. S6A (See Supporting Information). The inset gives the corresponding optical photograph of the wire. A hetero-interface is clearly observed with red emission on the left segment and blue emission on the right segment. Spatially resolved μ-PL measurements of an individual wire were performed on a confocal microscope system, as schematically shown in Fig. S6B and Fig. S7 (See Supporting Information). Dark-field emission images and PL spectra are shown in Fig. S6C and S6D at three representative positions (P_1-P_3) on the wire as indicated in A. It can be seen that positions P_1 and P_3 show strong emissions with peak centered at about 698 nm and 417 nm (P_1 and P_3 in Fig. S6D), respectively, which agree well with the band gap of $CsPbI_3$ (1.79 eV) and $CsPbCl_3$ (2.98 eV) [43–45], accordingly. At position P_2, where we expect the $CsPbI_3$/$CsPbCl_3$ hetero-interface is located, both the 417 nm and 698 nm emission peaks are simultaneously observed. These two peaks can be attributed to the emissions from $CsPbCl_3$ and $CsPbI_3$ at the heterojunction region [46]. Notably, no obvious defect-state related emissions are identified across the entire wire, nor at the hetero-interface region in Fig. S6D (See Supporting Information), indicating that these heterostructure nanowires have high crystallinity without any observable optically active defects. All these results agree perfectly well with the structural observation in displayed in Fig. 1.

2D PL mapping and spectra along the length of the wire are systematically investigated. PL mapping image of the heterostructure nanowire are presents in Fig. S6E (See Supporting Information). The individual emission-band (blue, 413–421 nm; red, 694–702 nm) of PL mapping (Fig. S6F and S6G, See Supporting Information) and the corresponding PL spectra (Fig. S6H and S6I, See Supporting Information) clearly show that the left and the right parts of the nanowire correspond to the $CsPbI_3$ (red) and $CsPbCl_3$ (blue) segment, respectively. The spatially resolved μ-PL results are in perfect agreement with the compositional measurements results (Fig. 1) and provide a direct proof that an axial heterojunction nanowire with two different perovskites are successfully realized using a sample CVD method. Notably, after the further optimization of growth conditions, for example, the growth time, carrier gas concentration, and pressure, the $CsPbCl_3$/$CsPbI_3$ nanowire heterojunctions with well-proportioned diameters are obtained, as

shown in Fig. S8 and S9 (See Supporting Information). Under the optical microscope, these wires show distinct black ($CsPbI_3$) and light ($CsPbCl_3$) segments on either side of the abrupt junction. A 2D PL mapping with corresponding spectra along a typical wire is shown in Fig. S9 (See Supporting Information) and illustrates that a near-perfect heterostructure with an abrupt interface is obtained.

The synthesis of nanowires with superlattice structures or multi-heterojunctions by a traditional CVD approach is a formidable challenge in nanotechnology [47]. Here, we report the fabrication of multi-heterojunction $CsPbCl_3/CsPbI_3/CsPbCl_3$ nanowires via a temperature controlled two-step CVD strategy as shown in Fig. S2 and S10 (See Supporting Information). Fig. 2 A shows a SEM image of the multi-heterojunction nanowires on the SiO_2/Si substrate. The wires have a linear morphology with lengths of several tens of micrometers and diameter about 100–300 nm. Fig. 2B–E shows four typical optical photographs of the as-grown wires, from which nanowires with multi-junctions are obviously observed. In order to further investigate the optical property of these heterostructures, PL measurements on a representative wire with two junctions are systematically performed and results are shown in Fig. 2F–L. The 2D PL mapping and spectra along the length of the wire are shown in Fig. 2G-J. The individual emission-band (blue, 413–421 nm; red, 694–702 nm) of PL mapping (Fig. 2G and 2I) and the corresponding PL spectra (Figs. 2H and 2 J) clearly show that the wire has double heterojunctions with two emission segments (a wide and a narrow segments) which correspond to the $CsPbCl_3$ (wide segment) and $CsPbI_3$ (narrow segment), respectively. Dark-field emission images and spatially resolved μ-PL spectra are shown in Fig. 2 K and 2 L at eight representative positions (P_1-P_8) along the wire as indicated in Fig. 2F. It can be seen that positions P_1, P_6 and P_3, P_4, P_8 show strong emissions with a single peak centered at about 698 nm and 417 nm (Fig. 2 L), respectively, which agree well with the band gap of $CsPbI_3$ (1.79 eV) and $CsPbCl_3$ (2.98 eV), accordingly [43–45]. At positions P_2,

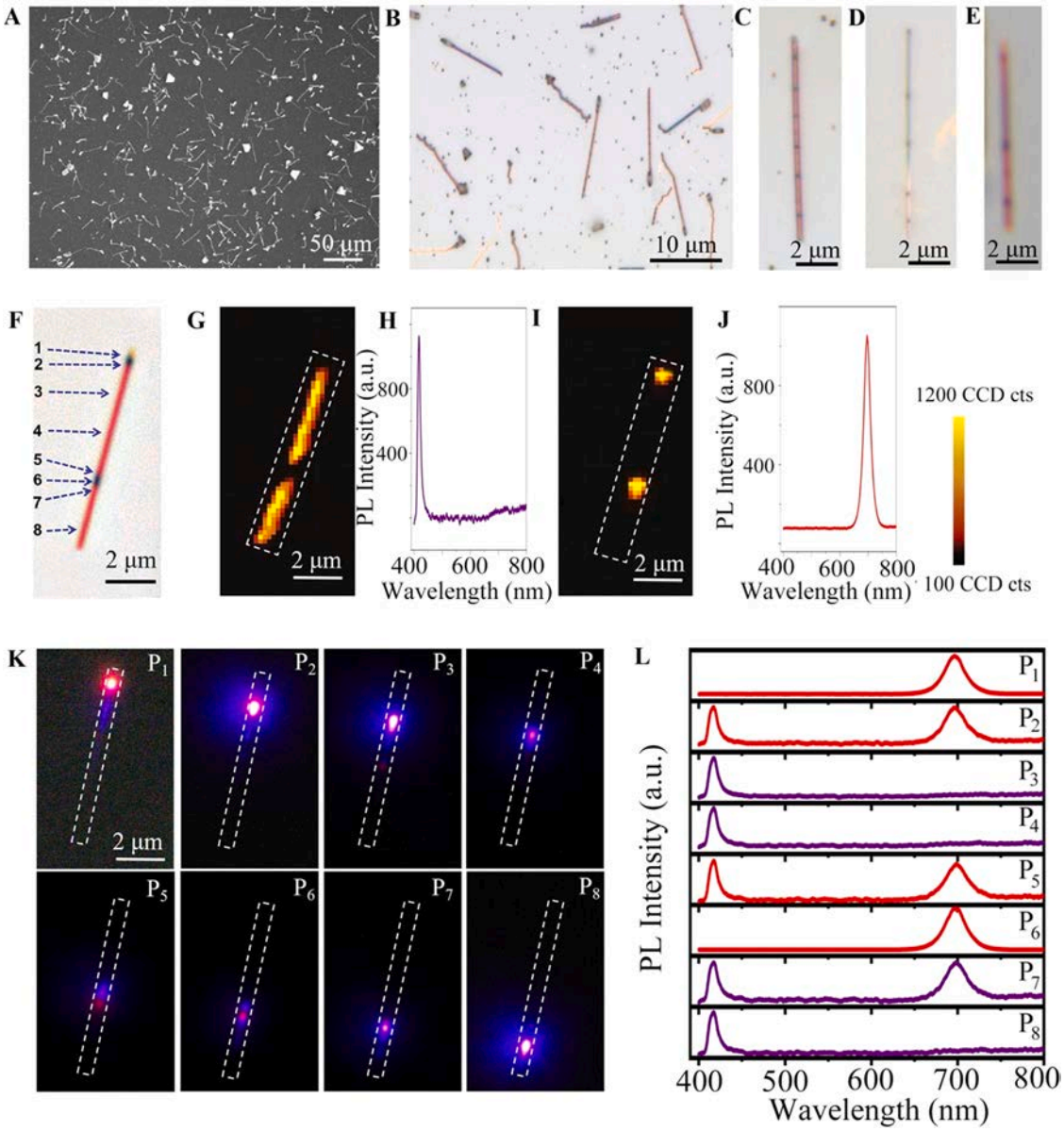

Fig. 2. Room-temperature optical characterization of typical multi-junction $CsPbCl_3/CsPbI_3/CsPbCl_3$ nanowires. (A) A low-resolution SEM image of the as-growth multi-junction nanowires. (B) An optical image of the heterostructure nanowires and (C-E) high-resolution photographs of three typical wires with various number of junctions. (F) A representative optical image of a heterostructure wire with two apparent junctions. (G-J) PL mapping images and spectra of the heterostructure wire. (G and I) 2D PL mapping images and the corresponding PL spectra (H and J) of a heterojunction nanowire in the regions of 413–421 nm and 694–702 nm, respectively. (K) A series of emission images (P_1-P_8) and (L) corresponding μ-PL spectra (P_1-P_8) along the axial direction, as indicated in (F).

P_5, and P_7, where we expect the $CsPbI_3/CsPbCl_3$ hetero-interfaces are located, both the 417 nm and 698 nm emission peaks are simultaneously observed without obvious defect-state related emissions. Furthermore, large-scale multi-heterojunction nanowire arrays on an annealed M-plane sapphire substrate are successfully realized as shown in Fig. 3. The schematic diagram of guided growth process is shown in Fig. 3 A. As can be seen, "V-shape" grooves are formed on the surface of M-plane sapphire after annealing, which acts as the guiding channels for nanowires. Fig. 3B shows the optical photograph of the M-plane sapphire after annealing. It can be seen that arrays of straight multi-heterojunction nanowire with a length of 10–20 μm grow along the "V-shape" grooves (Fig. 3C–H). These nanowire arrays also exhibit dual-wavelength emissions with blue and red bands, respectively, as presented in Fig. 3I–P. It is worth to note that the growth of these nanowire arrays are guided by catalysts on a 2 in. M-plane sapphire [48], where "V-shape" grooves emerged after annealing (Fig. 3C–E). Optical photographs of the guided multi-heterojunction nanowire arrays are nearly uniformly distributed from four different positions (Fig. S11A–D, See Supporting Information) of the whole 2-inch M-plane sapphire. Since such grooves are not formed on the C-plane sapphire or SiO_2/Si substrates, straight-shaped nanowire arrays cannot be fabricated, as shown in Fig. S12 (See Supporting Information), suggesting

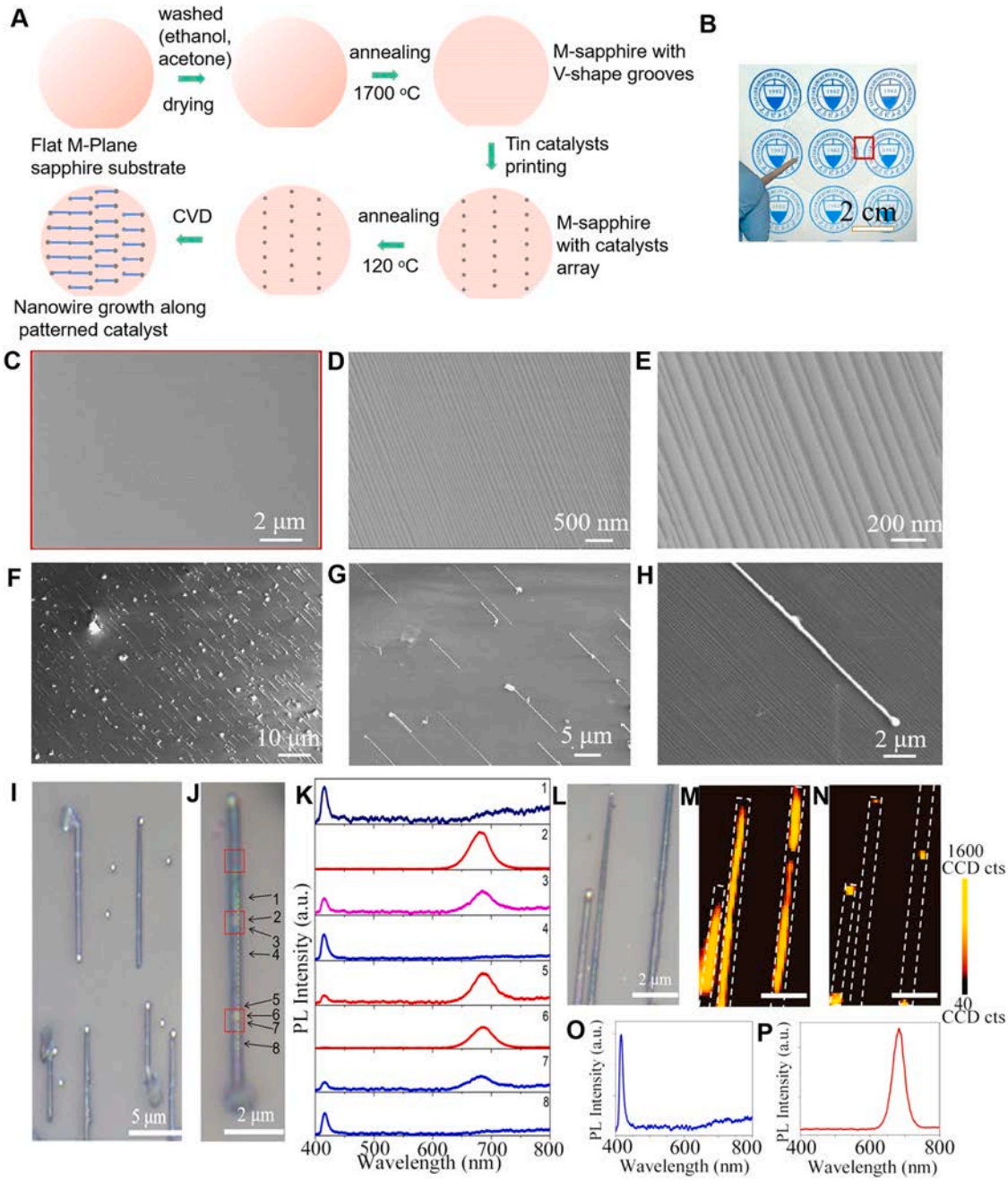

Fig. 3. Guided growth and optical characteristics of the multi-heterojunction nanowire arrays. (A) Schematic diagram of the guided growth process. (B) Optical photograph of the M-plane sapphire after annealing. (C) Low- and high-resolution (D,E) SEM images of the M-plane sapphire with V-shape grooves on the surface. (F-H) Low- and high-resolution SEM images of guided growth heterostructure nanowire arrays on the annealed M-plane sapphire substrate. (I,J) Optical images of the guided growth wires and corresponding PL spectra (1−8) (K) along a typical wire as indicated in (J). Red square indicates the positions of the heterojunctions. (L) Optical photograph of some selected wires, 2D PL mapping profiles (M,N) and the corresponding PL spectra (O,P) of the guided heterojunction nanowires in the regions of 413–421 nm and 678–686 nm, respectively.

that the "V-shape" grooves may play a key role during the guided growth. These unique heterostructure nanowires may provide material platforms for the optoelectronic integrated circuits.

Microstructural properties of these multi-heterojunction $CsPbCl_3$/$CsPbI_3$/$CsPbCl_3$ nanowires were studied by EDX and TEM. The elemental composition profiles of a representative nanowires with three heterojunctions are shown in Fig. S13 (See Supporting Information). The elemental maps and EDX spectra along the axial direction of the wire reveal that the junctions mainly consists of Pb, Cs, and I, while other parts primarily consists of Pb, Cs, and Cl, suggesting the formation of an abrupt multi-heterojunction wire here. Fig. 4A shows an optical image of some heterostructure nanowires (yellow square in A) on a copper grid, which are picked out from the primary substrate by 3D mechanical arms. Fig. 4B-D exhibit typical TEM images of a multi-heterojunction wire and a corresponding structural schematic diagram (4 C). The TEM image in Fig. 4D reveals a nanowire with a diameter of ~160 nm and length of ~5.5 μm. Two junctions (black segments) located at the middle parts of the wire can be seen on the wire, as indicated in Fig. 4D by blue arrows. Fig. 4E and F show the enlarged segment of the heterojunction (a black junction indicated by a blue arrow). Fig. 4G–I shows the high-resolution TEM (HRTEM) images taken from three positions along the heterojunction (indicated by "□", "○", and "△" in Fig. 4F), where a well-defined hetero-interface (indicated with a yellow line in Fig. 4H) is clearly observed. Across the junction, both the $CsPbCl_3$ and the $CsPbI_3$ maintain a single-crystalline structure. The measured lattice spacings in the $CsPbCl_3$ region and $CsPbI_3$ region are 0.397 nm and 0.891 nm, respectively, which are consistent with the (110) planes of orthorhombic phase $CsPbCl_3$ and $CsPbI_3$. These studies clearly demonstrate that high-quality $CsPbCl_3$/$CsPbI_3$/$CsPbCl_3$ multi-heterojunction nanowires are achieved with relatively sharp junction interfaces.

The axial heterostructure nanowires with excellent optical and electronic properties offer a robust material platforms for complex nanophotonics and functional optoelectronic devices [49,50]. Here, as an example, Fig. 5 shows the results of our investigation on an apparent asymmetrical optical waveguide behavior of a representative $CsPbCl_3$/$CsPbI_3$ heterostructure nanowire. Fig. 5A shows the schematic

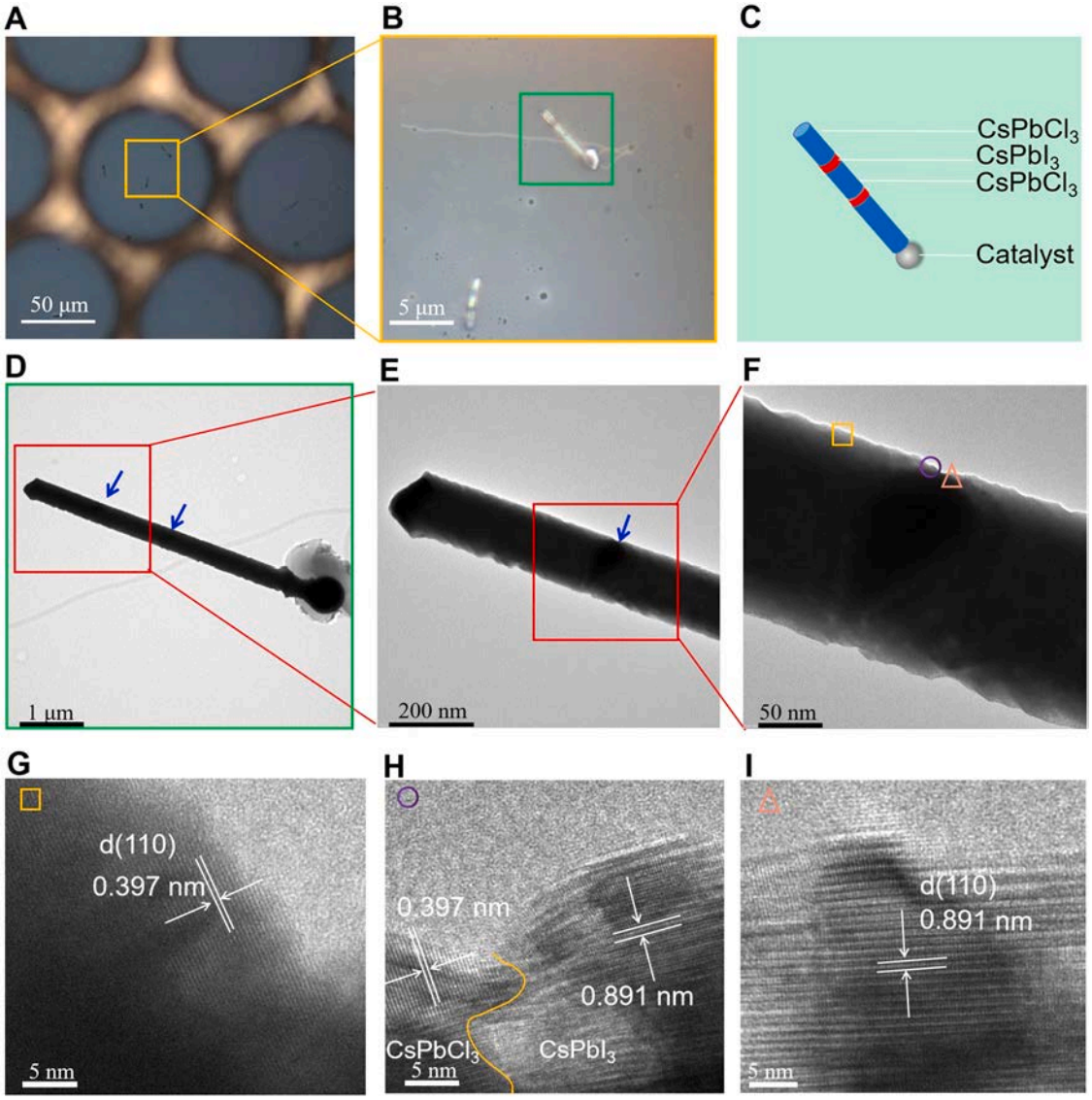

Fig. 4. (A) An optical image of some $CsPbCl_3$/$CsPbI_3$/$CsPbCl_3$ heterostructure nanowires (yellow square in (A)) on a copper grid, which were transferred from the grown substrate by 3D mechanical arms with two fiber probes. (B) Optical image of the multi-heterojunction wire and corresponding structural schematic diagram (C) of a heterostructure nanowires. (D-F) Low resolution TEM images of the selected multi-heterojunction wire with the length ~5.5 μm and diameter ~160 nm (green square in (B)). Blue arrows in D and E indicate the positions of the heterojunctions. (G-I) HRTEM images of three typical positions on the heterojunction as indicated in (F).

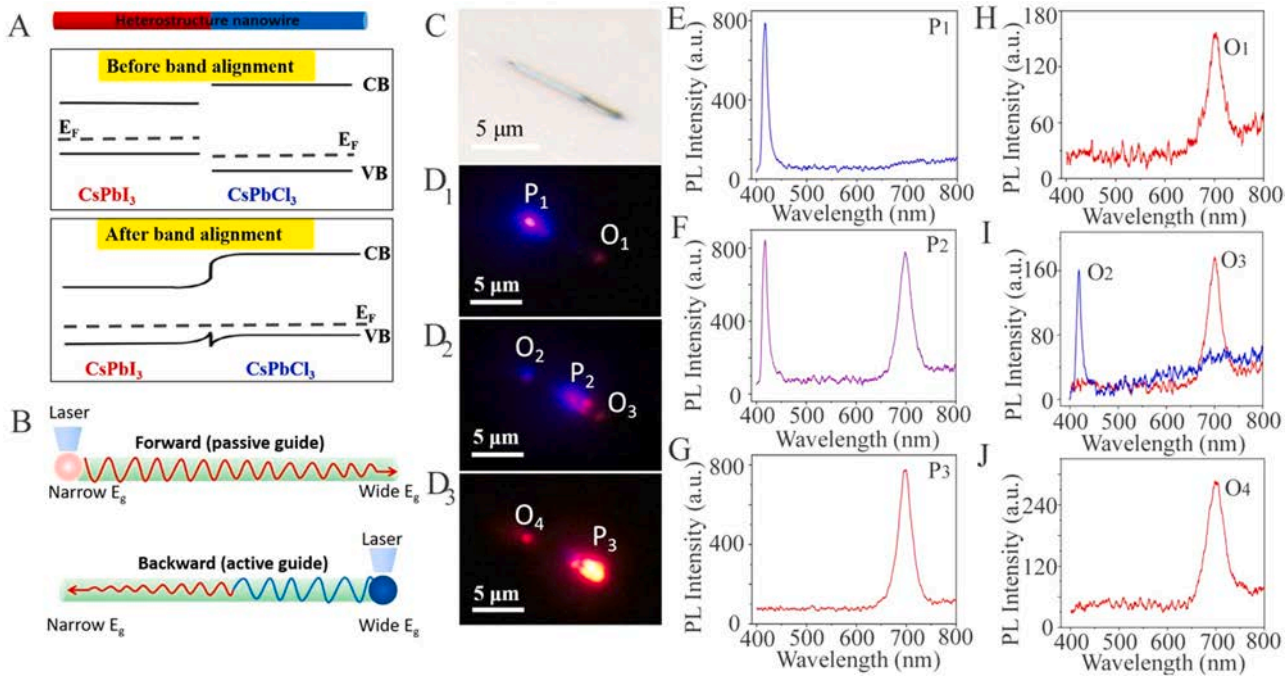

Fig. 5. Optical waveguide testing process of a single perovskite heterostructure nanowire with focused laser excitation. (A) Schematic diagram of an asymmetric perovskite heterostructure nanowire and its band structure along the axial direction before and after thermal equilibrium, respectively. (B) Schematic diagrams showing waveguiding effects with local excitation at the narrow- and wide-bandgap side of the NW, respectively. The emitted lights are actively or passively guided toward the two ends. (C) Optical image and (D) real-color photographs of a heterostructure wire under local light illumination by a same laser beam. (E–J) Corresponding PL spectra at the excitation position (P_1, P_2 and P_3) and the output ends (O_1, O_2, O_3 and O_4) of the heterostructure nanowire, respectively.

diagram of a perovskite heterostructure nanowire and the corresponding energy band diagram of the two perovskite materials before and after direct contact. When a focused laser shines at the narrow gap segment of the wire (Fig. 5B), the emitted light is expected to be passively guided (from $CsPbI_3$ to $CsPbCl_3$) along the wire through total internal reflections. In the reverse condition (from $CsPbCl_3$ to $CsPbI_3$), an active waveguide effect occurs along the wire through re-absorption and re-emission processes. To validate the above theoretical predictions, a $CsPbCl_3/CsPbI_3$ wire, which clearly exhibits two segments (dark and light) as shown in Fig. 5C, was removed from the substrate and dispersed onto a MgF_2 slide for careful optical investigations. The length and diameter of the wire are about 13 μm and 240 nm, respectively. Fig. 5 D_1–D_3 exhibits the corresponding PL images when it is locally excited by a focused laser beam (375 nm, spot size, ~1 μm) at the wire from the wide gap to narrow gap region (P_1-P_3). Obviously, a portion of the emitted light was guided by the wire cavity and leaks out at the ends of the nanowire (Fig. 5D). It is noted that the output signals at the opposite sides for the 3 cases are quite different in color, which may suggest an asymmetric optical guiding process. Moreover, the detected optical intensity from the narrow-band end is stronger than that of the wide-band end although the excited PL intensity is nearly the same, as shown in Fig. 5E–J, indicating the higher waveguiding efficiency of the former case. Fig. 5H–J shows the four output PL spectra (O_1-O_4) of the guided light, which quantitatively shows a ~2 fold maximum output intensity difference (O_1 versus O_4) after transporting through the entire 13 μm length. The guided light from wide gap to narrow gap also exhibits a red-shift of 23.5 meV when guided along the $CsPbCl_3/CsPbI_3$ wire due to the re-absorption and re-emitting processes. (Fig. S14, See Supporting Information). In particular, when the laser is locally irradiated at the junction of the wire (Fig. 5 D_2), the emitted light clearly shows asymmetric waveguide behavior, which are actively and passively guided toward the two ends (narrow gap and wide gap) of the wire, respectively. This way, the detected light from both ends present different colors (red and blue) with emitted wavelengths of about 419 nm and 699 nm (Fig. 5I).

Owing to the 1D geometry, the as-grown axial perovskite heterostructure wires would serve as a good waveguiding and oscillating cavity as well as an ideal gain material [51–55]. Moreover, these heterostructures have two emission bands (blue and red band), which are featured as the narrower-bandgap segment ($CsPbI_3$) and wide-bandgap segments ($CsPbCl_3$), respectively. The guided blue-light is actively transmitting through the $CsPbI_3$ segment via re-absorption and re-emission processes, while the guided red-light is passively propagating through the $CsPbCl_3$ segment. This asymmetric guiding process suggests that these heterostructure wires are ideal-model materials platform for investigating the interaction between the guiding light and perovskite wires. To demonstrate the quality of the waveguide and resonant cavity, pumping fluence-dependent room-temperature PL measurements were carried out using $CsPbCl_3/CsPbI_3$ wire as an example. Fig. 6 A shows a schematic diagram of the experimental setup for the measurement of the optically pumped nanowire lasers. The laser beam (400 nm, 150 fs, 1 kHz) was focused (spot size, ~50 μm) by an objective lens and then illuminated on the entire heterostructure wire. The local optical signals were detected at the wire end by a CCD spectrometer. Fig. 6B plots the pumping fluence dependent PL spectra from a typical $CsPbCl_3/CsPbI_3$ heterostructure (length: 12 μm and diameter: 220 nm). The wire exhibits two broad spontaneous emission bands respectively centered at 417 nm (blue-band) and 698 nm (red-band) at low pumping fluence (6.2 μJ cm^{-2}), corresponding to the emissions from $CsPbCl_3$ and $CsPbI_3$, respectively. When the pump fluence increases to ~ 16.0 μJ cm^{-2}, a sharp emission line appears at 687.4 nm. When the pumping fluence increases to ~24.4 μJ cm^{-2}, two additional emission lines in the blue band (425.5 nm and 423.2 nm) appear, which correspond to the Fabry-Perot (F-P) cavity modes. With further increase of the pumping fluence, the intensity of the modes at 687.4 nm and 425.5 nm enhances faster than other modes in the red and blue band. The threshold pump power density for the super-linear increase in emission intensity are ~24.4 μJ cm^{-2} and ~16.0 μJ cm^{-2} for the blue- and red-band, respectively (Fig. 6C). After examine a dozen of heterostructure wires, the obtained threshold ratio between these

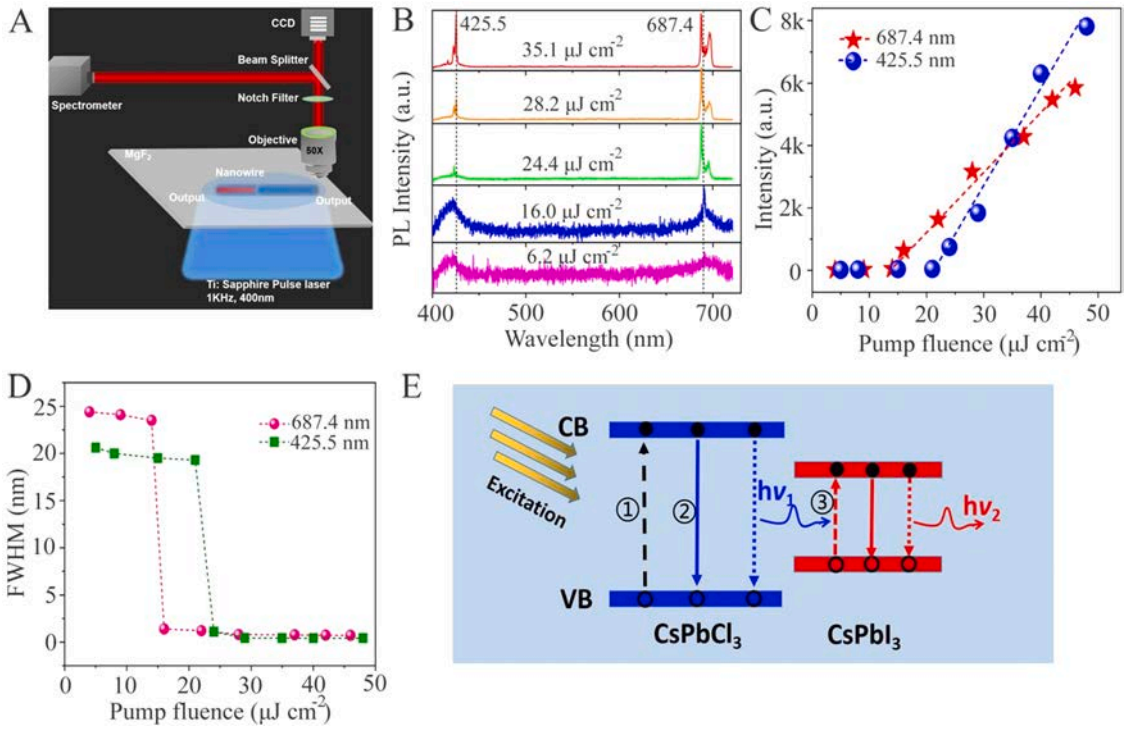

Fig. 6. (A) Schematic diagram of the experimental setup for the lasing measurements on a $CsPbCl_3/CsPbI_3$ heterostructure nanowire. The wire is under a wide illumination of a femtosecond laser. (B) Pumping power dependent room-temperature PL spectra of a typical $CsPbCl_3/CsPbI_3$ heterostructure nanowire. (C) Pumping fluence-dependent emission intensity at ~425.5 nm (blue-band, spheres) and at ~687.4 nm (red-band, stars), respectively. (D) Pumping fluence-dependent line width of a $CsPbCl_3/CsPbI_3$ wire for red-band (pink spheres) and blue-band (green squares). (E) A schematic band diagram showing carrier transfer processes for a $CsPbCl_3/CsPbI_3$ wire under a pulsed laser illumination. CB and VB refer to the conduction band and valence band, respectively. The solid and blank circles denote electrons and holes, respectively. ① Photogenerated carriers from band to band transitions. ② The electron-hole pairs recombined radiatively, resulting in emitted photons (luminescence). ③ The emitted higher energy photons ($h\nu_1$) could be reabsorbed by the $CsPbI_3$ with narrower bandgap followed by recombination and emission of lower energy photons ($h\nu_2$).

heterojunction wires usually has a value ranged from 0.2 to 0.6 depending on the quality of the wire cavities. Fig. 6D shows that the full width at half maximum (FWHM) of the emission peaks decrease drastically from about 20 nm (spontaneous emission) to sub-nanometer, ~0.78 nm and ~0.45 nm for the red and blue peaks, respectively, when the pump power reaches the respective threshold for the two bands (Fig. S15, See Supporting Information). This clearly indicates the occurrence of dual-wavelength stimulated emission within a single heterostructure wire. This can be further explained in the schematic band diagram in Fig. 6E, exhibiting carrier transfer processes for a $CsPbCl_3/CsPbI_3$ wire under a pulsed laser illumination. When the incident light falls on the wire with high pump levels, the photogenerated carriers from band to band transitions in the wide bandgap $CsPbI_3$ are shown in process (①). The electron-hole pairs recombined radiatively, resulting in the emitted photon (luminescence) (process (②)). The emitted higher energy photons ($h\nu_1$) could be reabsorbed by $CsPbI_3$ with the narrower band gap (③) followed by recombination and emission of lower energy photons ($h\nu_2$). In addition, it is worth mentioning that with the increase of the pumping fluence, the emission peaks in the red-band show a slight blue-shift of ~2.4 nm, while the emission wavelengths at blue-band are constant. This difference in the spectral shift may come from the higher carrier density in $CsPbI_3$ than that of $CsPbCl_3$ due to carrier transfer from the later to the former ones [56]. These results clearly demonstrate that the $CsPbCl_3/CsPbI_3$ heterostructure wires can confine a dual-wavelength lasing, which can provide the model-material platform for the development on multicolor displays.

4. Conclusion

In conclusion, high-quality $CsPbCl_3/CsPbI_3$ axial heterostructure nanowires and multi-heterojunction nanowires were synthesized through a temperature controlled multi-step solid-source CVD strategy. Microstructural, chemical and optical characterization reveal that these wires have a single-crystalline structure with abrupt interfaces at the junctions with low defect density. PL mapping at the heterojunctions exhibit dual-wavelength emission bands, from the two adjacent disparate perovskites, which further demonstrate the formation of unique heterostructures. Moreover, the asymmetrical waveguide behavior and the construction of a monolithic dual-color laser with blue and red emission bands using an on-wire axial perovskite heterostructure nanowire are realized successfully. These achievements represent a significant advance in the controllable synthesis of axial perovskite heterostructures, which may have potential applications in highly integrated photonic and optoelectronic devices.

CRediT authorship contribution statement

Pengfei Guo: Conceptualization, Data curation, Formal analysis, Funding acquisition, Investigation, Methodology, Writing – original draft, Supervision, Project administration. **Da Liu:** Data curation, Formal analysis. **Xia Shen:** Methodology, Data curation, Formal analysis. **Qihang Lv:** Data curation, Resources. **Yu Wu:** Methodology, Resources. **Qian Yang:** Methodology, Resources. **Pu Li:** Resources. **Yuying Hao:** Resources. **Johnny C. Ho:** Project administration. **Kin Man Yu:** Supervision, Project administration, Writing – review & editing.

Declaration of Competing Interest

The authors declare that they have no known competing financial interests or personal relationships that could have appeared to influence

the work reported in this paper.

Acknowledgement

The authors are grateful to the start-up funding from Taiyuan University of Technology and Shanxi Basic Research Program Project (No. 20210302123128) for financial support. KMY acknowledges support of the CityU SGP (Grant No. 9380076). JCH acknowledges support from General Research Fund (CityU 11306520) of the Research Grants Council of Hong Kong SAR, China..

Appendix A. Supporting information

Supplementary data associated with this article can be found in the online version at doi:10.1016/j.nanoen.2021.106778.

References

[1] W. Nie, H. Tsai, R. Asadpour, J. Blancon, A. Neukirch, G. Gupta, J. Crochet, M. Chhowalla, S. Tretiak, M. Alam, H. Wang, A.D. Mohite, High-efficiency solution-processed perovskite solar cells with millimeter-scale grains, Science 347 (2015) 522–525.
[2] J. Burschka, N. Pellet, S. Moon, R.H. Baker, P. Gao, M.K. Nazeeruddin, M. Grätzel, Sequential deposition as a route to high-performance perovskite-sensitized solar cells, Nature 499 (2013) 316–319.
[3] Y.L. Wang, X. Guan, D.H. Li, H. Cheng, X.D. Duan, Z.Y. Lin, X.F. Duan, Chemical vapor deposition growth of single-crystalline cesium lead halide microplatelets and heterostructures for optoelectronic applications, Nano Res 10 (2017) 1223.
[4] S.T. Ha, R. Su, J. Xing, Q. Zhang, Q.H. Xiong, Metal halide perovskite nanomaterials: synthesis and applications, Chem. Sci. 8 (2017) 2522–2536.
[5] Y.P. Fu, T. Wu, J. Wang, J.Y. Zhai, M.J. Shearer, Y.Z. Zhao, R.J. Hamers, E. Kan, K. M. Deng, X.Y. Zhu, S. Jin, Stabilization of the metastable lead iodide perovskite phase via surface functionalization, Nano Lett. 17 (2017) 4405.
[6] J.L. Xu, X.Y. Li, J.B. Xiong, C.Q. Yuan, S. Semin, T. Rasing, X.H. Bu, Halide perovskites for nonlinear optics, Adv. Mater. 32 (2020) 1806736.
[7] Q. Zhang, R. Su, X.F. Liu, J. Xing, T.C. Sum, Q.H. Xiong, High-quality whispering-gallery-mode lasing from cesium lead halide perovskite nanoplatelets, Adv. Funct. Mater. 26 (2016) 6238.
[8] W. Li, Z. Wang, F. Deschler, S. Gao, R.H. Friend, A.K. Cheetham, Chemically diverse and multifunctional hybrid organic–inorganic perovskites, Nat. Rev. Mater. 2 (2017) 16099.
[9] T.M. Brenner, D.A. Egger, L. Kronik, G. Hodes, D. Cahen, Hybrid organic-inorganic perovskites: low-cost semiconductors with intriguing charge-transport properties, Nat. Rev. Mater. 1 (2016) 15007.
[10] N.J. Jeon, J.H. Noh, W.S. Yang, Y.C. Kim, S. Ryu, J. Seo, S.I. Seok, Compositional engineering of perovskite materials for high performance solar cells, Nature 517 (2015) 476–480.
[11] L. Protesescu, S. Yakunin, M.I. Bodnarchuk, F. Krieg, R. Caputo, C.H. Hendon, R. X. Yang, A. Walsh, M.V. Kovalenko, Nanocrystals of cesium lead halide perovskites ($CsPbX_3$, X=Cl, Br, and I): novel optoelectronic materials showing bright emission with wide color gamut, Nano Lett. 15 (2015) 3692–3696.
[12] D. Zhang, S.W. Eaton, Y. Yu, L. Dou, P. Yang, Solution-phase synthesis of cesium lead halide perovskite nanowires, J. Am. Chem. Soc. 137 (2015) 9230–9233.
[13] L.T. Dou, M.L. Lai, C.S. Kley, Y.M. Yang, C.G. Bischak, D.D. Zhang, S.W. Eaton, N. S. Ginsberg, P.D. Yang, Spatially resolved multicolor $CsPbX_3$ nanowire heterojunctions via anion exchange, Proc. Natl. Acad. Sci. USA 114 (2017) 7216.
[14] K. Park, J.W. Lee, J.D. Kim, N.S. Han, D.M. Jang, S. Jeong, J. Park, J.K. Song, J. Phys. Chem. Lett. 7 (2016) 3703.
[15] Q.A. Akkerman, V. Innocenzo, S. Accornero, A. Scarpellini, A. Petrozza, M. Prato, L. Manna, Tuning the optical properties of cesium lead halide perovskite nanocrystals by anion exchange reactions, J. Am. Chem. Soc. 137 (2015) 10276–10281.
[16] G. Xing, N. Mathews, S.S. Lim, N. Yantara, X.F. Liu, D. Sabba, M. Grätzel, S. Mhaisalkar, T.C. Sum, Low-temperature solution-processed wavelength-tunable perovskites for lasing, Nat. Mater. 13 (2014) 476.
[17] Q. Zhang, Q. Shang, R. Su, T.T. Do, Q.H. Xiong, Halide perovskite semiconductor lasers: materials, cavity design, and low threshold, Nano Lett. 21 (2021) 1903–1914.
[18] M. Lu, Y. Zhang, S. Wang, J. Guo, W.W. Yu, A.L. Rogach, Metal halide perovskite light-emitting devices: promising technology for next-generation displays, Adv. Funct. Mater. 29 (2019) 1902008.
[19] P.F. Guo, M.K. Hossain, X. Shen, H. Sun, W. Yang, C. Liu, C.Y. Ho, C.K. Kwok, S. Tsang, Y. Luo, J.C. Ho, K.M. Yu, Room-temperature Red–Green–Blue whispering-gallery mode lasing and white-light emission from cesium lead halide perovskite ($CsPbX_3$, X=Cl, Br, I) microstructures, Adv. Opt. Mater. 6 (2018) 1700993.
[20] J. Chen, Y. Fu, L. Samad, L. Dang, Y. Zhao, S. Shen, L. Guo, S. Jin, Vapor-phase epitaxial growth of aligned nanowire networks of cesium lead halide perovskites ($CsPbX_3$, X =Cl, Br, I), Nano Lett. 17 (2017) 460–466.
[21] E. Shi, B. Yuan, S.B. Shiring, Y. Gao, Akriti, Y. Guo, C. Su, M. Lai, P.D. Yang, J. Kong, B.M. Savoie, Y. Yu, L.T. Dou, Two-dimensional halide perovskite lateral epitaxial heterostructures, Nature 580 (2020) 614–620.
[22] Y.P. Fu, H.M. Zhu, C.C. Stoumpos, Q. Ding, J. Wang, M.G. Kanatzidis, X. Zhu, S. Jin, Broad wavelength tunable robust lasing from single-crystal nanowires of cesium lead halide perovskites ($CsPbX_3$, X = Cl, Br, I), ACS Nano 10 (2016) 7963–7972.
[23] S. Yakunin, M.I. Bodnarchuk, M.J. Grotevent, Anion-exchange in highly luminescent nanocrystals of cesium lead halide perovskites ($CsPbX_3$, X = Cl, Br, I), Nano Lett. 15 (2015) 5635–5640.
[24] M.K. Hossain, P.F. Guo, W. Qarony, Y.H. Tsang, C. Liu, S.W. Tsang, J.C. Ho, K. M. Yu, Controllable optical emission wavelength in all-inorganic halide perovskite alloy microplates grown by two-step chemical vapor deposition, Nano Res. 13 (2020) 2939–2949.
[25] Y. Meng, C. Lan, F. Li, S.P. Yip, R. Wei, X. Kang, X. Bu, R. Dong, H. Zhang, J.C. Ho, Direct vapor-liquid-solid synthesis of all-Inorganic perovskite nanowires for high-performance electronics and optoelectronics, ACS Nano 13 (2019) 6060–6070.
[26] J. Xing, X.F. Liu, Q. Zhang, S.T. Ha, Y.W. Yuan, C. Shen, T.C. Sum, Q.H. Xiong, Vapor phase synthesis of organometal halide perovskite nanowires for tunable room-temperature nanolasers, Nano Lett. 15 (2015) 4571–4577.
[27] B. Tang, H. Dong, L. Sun, W. Zheng, Q. Wang, F. Sun, X. Jiang, A. Pan, L. Zhang, Single-mode lasers based on cesium lead halide perovskite submicron spheres, ACS Nano 11 (2017) 10681–10688.
[28] T. Lei, M. Lai, Q. Kong, D. Lu, W. Lee, L. Dou, V. Wu, Y. Yu, P.D. Yang, Electrical and optical tunability in all Inorganic halide perovskite alloy nanowires, Nano Lett. 18 (2018) 3538–3542.
[29] P. Liu, X. He, J. Ren, Q. Liao, J.N. Yao, H.B. Fu, Organic−inorganic hybrid perovskite nanowire laser arrays, ACS Nano 11 (2017) 5766–5773.
[30] J. Feng, X. Yan, Y. Zhang, X. Wang, Y. Wu, B. Su, H.B. Fu, L. Jiang, "Liquid knife" to fabricate patterning single-crystalline perovskite microplates toward high-performance laser arrays, Adv. Mater. 28 (2016) 3732–3741.
[31] J. Xing, F. Yan, Y.W. Zhao, S. Chen, H.K. Yu, Q. Zhang, R.G. Zeng, H.V. Demir, X. W. Sun, A. Huan, High-efficiency light-emitting diodes of organometal halide perovskite amorphous nanoparticles, ACS Nano 10 (2016) 6623–6630.
[32] Y.C. Ling, Y. Tian, X. Wang, J.C. Wang, J.M. Knox, F. Perez-Orive, Y. Du, L. Tan, K. Hanson, B. Ma, H. Gao, Enhanced optical and electrical properties of polymer-assisted all-inorganic perovskites for light-emitting diodes, Adv. Mater. 28 (2016) 8983–8989.
[33] Y. Wang, C. Jia, Z. Fan, Z. Lin, S. Lee, T.L. Atallah, J.R. Caram, Y. Huang, X. F. Duan, Large-area synthesis and patterning of all-Inorganic lead halide perovskite thin films and heterostructures, Nano Lett. 21 (2021) 1454–1460.
[34] Y. Wang, Z. Chen, F. Deschler, X. Sun, T. Lu, E.A. Wertz, J. Hu, J. Shi, Epitaxial halide perovskite lateral double heterostructure, ACS Nano 11 (2017) 3355–3364.
[35] Q. Ba, A. Jana, L. Wang, K.S. Kim, Dual emission of water-stable 2D organic–inorganic halide perovskites with Mn(II) dopant, Adv. Funct. Mater. 29 (2019) 1904768.
[36] Y. Xiao, C. Meng, P. Wang, Y. Ye, H.K. Yu, S.S. Wang, F.X. Gu, L. Dai, L.M. Tong, Single-nanowire single-mode laser, Nano Lett. 11 (2011) 1122–1128.
[37] Q. Liao, X. Guo, S. Lv, Z.Z. Xu, Y. Zhang, H.B. Fu, Cluster-mediated nucleation and growth of H-type polymorphs of difluoroboron avobenzone for organic microribbon lasers, ACS Nano 12 (2018) 5359–5367.
[38] N.P. Dasgupta, J. Sun, C. Liu, S. Brittman, S.C. Andrews, J. Lim, H. Gao, R. Yan, P. D. Yang, 25th anniversary article: semiconductor nanowires–synthesis, characterization, and applications, Adv. Mater. 26 (2014) 2137–2184.
[39] S. Lepri, G. Casati, Asymmetric wave propagation in nonlinear systems, Phys. Rev. Lett. 106 (2011) 164101–164104.
[40] P.F. Guo, J.Y. Xu, K. Gong, X. Shen, Y. Lu, Y. Qiu, J.Q. Xu, Z.J. Zou, C.L. Wang, H. L. Yan, Y.S. Luo, A.L. Pan, H. Zhang, J.C. Ho, K.M. Yu, On-nanowire axial heterojunction design for high-performance photodetectors, ACS Nano 10 (2016) 8474–8480.
[41] S. Makarov, A. Furasova, E. Tiguntseva, A. Hemmetter, A. Berestennikov, A. Pushkarev, A. Zakhidov, Y. Kivshar, Halide-perovskite resonant nanophotonics, Adv. Opt. Mater. 7 (2019) 1800784.
[42] L.N. Quan, J. Kang, C.Z. Ning, P.D. Yang, Nanowires for photonics, Chem. Rev. 119 (2019) 9153–9169.
[43] M. Sebastian, J.A. Peters, C.C. Stoumpos, J. Im, S.S. Kostina, Z. Liu, M. G. Kanatzidis, A.J. Freeman, B.W. Wessels, Excitonic emissions and above-band-gap luminescence in the single-crystal perovskite, semiconductors CsPbBr3 and CsPbCl3, Phys.Rev. B 92 (2015), 235210.
[44] Z. Zhou, Y. Cui, H. Deng, L. Huang, Z. Wei, J.B. Li, Modulation of electronic and optical properties in mixed halide perovskites CsPbCl3xBr3(1-x) and CsPbBr3xI3 (1-x), Appl. Phys. Lett. 110 (2017), 113901.
[45] R.A. Evarestov, E.A. Kotomin, A. Senocrate, R.K. Kremer, J. Maier, First-principles comparative study of perfect and defective CsPbX 3 (X= Br, I) crystals, Phys. Chem. Chem. Phys. 22 (2020) 3914–3920.
[46] Z. Zhang, L. Shen, Y. Zhao, Y. Zhang, H. Yang, W. Xiang, X. Liang, G. Chen, H. Yu, Coexisting $CsPbCl_3$:$CsPbI_3$ perovskite nanocrystal glasses with high luminescence and stability, Chem. Eng. J. 385 (2020), 123415.
[47] C.C. Jia, Z.Y. Lin, Y. Huang, X.F. Duan, Nanowire electronics: from nanoscale to macroscale, Chem. Rev. 119 (2019) 9074–9135.
[48] D. Tsivion, M. Schvartzman, R. Popovitz-Biro, P. Huth, E. Joselevich, Guided growth of millimeter-long horizontal nanowires with controlled orientations, Science 333 (2011) 1003–1007.
[49] Q. Kong, W. Lee, M. Lai, C.G. Bischak, G. Gao, A.B. Wong, T. Lei, Y. Yu, L. Wang, N. S. Ginsberg, P.D. Yang, Phase-transition–induced p-n junction in single halide perovskite nanowire, Proc. Natl. Acad. Sci. USA 115 (2018) 8889–8894.
[50] L. Huang, Q. Gao, L. Sun, H. Dong, S. Shi, T. Cai, Q. Liao, C. Yan, Composition-graded cesium lead halide perovskite nanowires with tunable dual-color lasing performance, Adv. Mater. 30 (2018) 1800596.

[51] S.W. Eaton, M. Lai, N.A. Gibson, A.B. Wong, L. Dou, J. Ma, L. Wang, S.R. Leone, P. D. Yang, Lasing in robust cesium lead halide perovskite nanowires, Proc. Natl. Acad. Sci. USA 8 (2016) 1993–1998.
[52] H. Zhu, Y. Fu, F. Meng, X. Wu, Z. Gong, Q. Ding, M.V. Gustafsson, M. Tuan Trinh, S. Jin, X.Y. Zhu, Lead halide perovskite nanowire lasers with low lasing thresholds and high quality factors, Nat. Mater. 14 (2015) 636–642.
[53] C.Z. Ning, L. Dou, P.D. Yang, Bandgap engineering in semiconductor alloy Nanomaterials with widely tunable compositions, Nat. Rev. Mater. 2 (2017) 17070.
[54] Y. Fu, H. Zhu, J. Chen, M.P. Hautzinger, X.Y. Zhu, S. Jin, Metal halide perovskite nanostructures for optoelectronic applications and the study of physical properties, Nat. Rev. Mater. 4 (2019) 169–188.
[55] Q. Zhang, R. Su, W. Du, X. Liu, L. Zhao, S.T. Ha, Q.H. Xiong, Advances in small perovskite-based lasers, Small, Methods 1 (2017) 1700163.
[56] Q.L. Zhang, H. Liu, P.F. Guo, D. Li, P. Fan, W. Zheng, X. Zhu, Y. Jiang, H. Zhou, W. Hu, X. Zhuang, H. Liu, X.F. Duan, A. Pan, Vapor growth and interfacial carrier dynamics of high-quality CdS-CdSSeCdS axial nanowire heterostructures, Nano Energy 32 (2017) 28–35.

Dr. Pengfei Guo received his Ph.D. from the College of Materials Science and Engineering at Hunan University. From 2016–2018, he worked as a Postdoctoral Research Fellow in City University of Hong Kong. In 2019, he joined the College of Physics and Optoelectronics in Taiyuan University of Technology as an associate professor. His research interests include the synthesis of the low-dimensional semiconductor material with controlled CVD route, and their applications in future electronics, photonics and energy technologies.

Da Liu received his BS in material from North University of China. He is currently studying in physics as a master in Taiyuan University of Technology, China. His main research interests are perovskite nanomaterials, heterostructures as well as their applications to nano-laser and optoelectronics.

Xia Shen received her Master degree in physics and electronics from East China Normal University. She is currently a teaching assistant in the Key Laboratory of Advanced Transducers and Intelligent Control System Ministry of Education, Taiyuan University of Technology. Her main research interests are the ultrafast photoluminescence spectroscopy, semiconductor nanomaterials and their application in photoelectric devices.

Qihang Lv received his BS in physics from Jinzhong University of China. He is currently studying in physics as a master in Taiyuan University of Technology, China. His main research interests are one-dimensional nanomaterials as well as their applications to detectors and nano-lasers.

Yu Wu received his BS in physics from Harbin Institute of Technology of China. He is currently studying in physics as a master in Taiyuan University of Technology, China. His main research interests are the ultrafast photoluminescence spectroscopy of the semiconductor materials.

Qian Yang received her BS in physics from Xihua University of China. She is currently studying in physics as a master in Taiyuan University of Technology, China. Her main research interests are one-dimensional nanomaterials as well as their applications to high-performance photodetectors.

Prof. Pu Li is a full professor at Taiyuan University of Technology. His research interests focus on the optics and ultrafast physics. He has published more than 50 papers.

Prof. Yuying Hao is a full professor at Taiyuan University of Technology. Her research interests focus on the materials design for energy storage and conversion. She has published more than 100 papers.

Prof. Johnny C. Ho obtained his B.S. in chemical engineering with high honors from the University of California at Berkeley in 2002. He then received his M.S. and Ph.D. in materials science and engineering from the University of California at Berkeley in 2005 and 2009, respectively, specializing in the topic of design of nano-materials for next-generation electronics under the supervision of Professor Ali Javey in electrical engineering. His research interest is highly interdisciplinary involving chemistry, physics, materials science and various engineering disciplines to explore novel nanomaterials and nano-engineering techniques for technological applications.

Prof. Kin Man Yu is a full professor at City University of Hong Kong. He has coauthored 12 book chapters and invited reviews, published over 400 journal articles with over 10000 citations, and co-authored several patents related to advanced PV technology. In 2006, Dr. Yu received an R&D 100 award (Editor's choice for most promising technology) for his work with Dr. Wladek Walukiewicz on multiband semiconductors for high efficiency solar cells. Since August 2014, he serves as an Associate Editor for the Journal of Applied Physics.